A rapid numerical method for solving Serre-Green-Naghdi equations describing long free surface gravity waves

N Favrie, S Gavrilyuk

A rapid numerical method for solving Serre-Green-Naghdi equations describing long free surface gravity waves

N. Favrie*, S. Gavrilyuk†

May 22, 2017

Abstract

A new numerical method for solving the Serre-Green-Naghdi (SGN) equations describing dispersive waves on shallow water is proposed. From the mathematical point of view, the SGN equations are the Euler-Lagrange equations for a 'master' lagrangian submitted to a differential constraint which is the mass conservation law. One major numerical challenge in solving the SGN equations is the resolution of an elliptic problem at each time instant. This is the most time-consuming part of the numerical method. The idea is to replace the 'master' lagrangian by a one-parameter family of 'augmented' lagrangians, depending on a greater number of variables, for which the corresponding Euler - Lagrange equations are hyperbolic. In such an approach, the 'master' lagrangian is recovered by the augmented lagrangian in some limit (for example, when the corresponding parameter is large). The choice of such a family of augmented lagrangians is proposed and discussed. The corresponding hyperbolic system is numerically solved by a Godunov type method. Numerical solutions are compared with exact solutions to the SGN equations. It appears that the computational time in solving the hyperbolic system is much lower than in the case where the elliptic operator is inverted. The new method is applied, in particular, to the study of 'Favre waves' representing non-stationary undular bores produced after reflection of the fluid flow with a free surface at an immobile wall.

Keywords: dispersive equations, hyperbolicity, Godunov type methods

1 Introduction

Dispersive systems of equations appearing in physics often admit a variational formulation. Numerous physical examples can be found in the literature : water waves, quantum mechanics, solid mechanics, capillary fluids, bubbly fluids, etc. (cf. [32], [1], [30], [8], [2], [15]). Even if the physics is better captured by the dispersive models, the mathematical and numerical study of such models represents a difficult problem. One example is the Serre-Green-Naghdi equations (SGN equations) describing dispersive water waves [27], [17], [18], [29]. In particular, the inversion of an elliptic operator is needed at each time step when the model is numerically solved [20], [22]. As a consequence, this drastically increases the calculation time. An analogous approach was also applied in [25] for a linearised version of the SGN equations (Boussinesq equations).

*Aix-Marseille Université, UMR CNRS 7343, IUSTI, 5 rue E. Fermi, 13453 Marseille Cedex 13, France, nicolas.favrie@univ-amu.fr

†Corresponding author : Aix-Marseille Université, UMR CNRS 7343, IUSTI, 5 rue E. Fermi, 13453 Marseille Cedex 13, France and Novosibirsk State University, 2 Pirogova street, 630090 Novosibirsk, Russia, sergey.gavrilyuk@univ-amu.fr

Another important numerical problem is how to impose artificial non-reflecting (transparent) conditions at the boundary of the calculation region for dispersive equations. The transparent boundary conditions are important when one looks for waves passing through a bounded numerical domain. This is always an open problem for general dispersive equations. Some progress was recently done for scalar dispersive equations (Korteweg-de Vries and Benjamin-Bona-Mahony equations) [3], [4]. However, in the theory of hyperbolic equations the last question is solved, at least for homogeneous systems of equations (see [19], for example). Indeed, to avoid the wave reflection, it is necessary just to 'kill' the Riemann invariants corresponding to the characteristics which enter the domain of calculation. A natural idea is thus to replace dispersive equations by approximate hyperbolic equations. The idea is not new and comes from the pioneering work by Cattaneo [5] who replaced, in particular, the heat equation by a hyperbolic system of equations with relaxation. A recent important development of such an approach to dissipative continuum mechanics models can be found in [26] and [7]. However, such an approach can not be satisfactory when the governing system are the Euler-Lagrange equations for some lagrangian (below called 'master' lagrangian). Indeed, the energy should be conserved, while it decreases when the classical dissipation-type relaxation is added. An idea consists to consider an approximative lagrangian (below called 'augmented' lagrangian) where some gradients or temporal derivatives of unknowns are replaced by new variables that become true gradients or temporal derivatives only in some limit. Such a limit is not a viscous Cattaneo type limit, because the energy of the system is conserved, but a 'non-viscous' limit allowing us to 'spread' the energy of the 'master' system into additional degrees of freedom. To understand the idea of such a construction let us first give a simple example coming from the ODE. Consider a master Lagrangian describing free oscillations $x(t)$ of a mass point :

$$L = \left(\frac{dx}{dt}\right)^2 - \frac{x^2}{2} \tag{1}$$

An augmented Lagrangian where a new time dependent variable y is added, is taken in the form:

$$\hat{L} = \left(\frac{dy}{dt}\right)^2 - \frac{x^2}{2} - \lambda\frac{(y-x)^2}{2}. \tag{2}$$

Here λ is a large parameter. The Euler-Lagrange equations for (2) are :

$$\frac{d^2y}{dt^2} + \lambda(y-x) = 0, \quad -x + \lambda(y-x) = 0.$$

The solution $y(t,\lambda)$ of the Cauchy problem $y(0,\lambda) = A$, $\dot{y}(0,\lambda) = B$ is :

$$y(t,\lambda) = \sqrt{A^2 + \frac{B^2}{\omega^2}}\sin\left(\omega t + \varphi_\lambda\right),\ \varphi_\lambda = \arcsin\left(A/\sqrt{A^2 + \frac{B^2}{\omega^2}}\right),\ \omega^2 = \frac{\lambda}{1+\lambda},$$

while the solution $x(t)$ corresponding to the master Lagrangian (1) with the same initial data is :

$$x(t) = \sqrt{A^2 + B^2}\sin\left(t + \varphi\right),\ \varphi = \arcsin\left(A/\sqrt{A^2 + B^2}\right).$$

The approximate solution $y(t,\lambda)$ and exact solution $x(t)$ remain close to each other as $\lambda \to \infty$ in the sense that their amplitudes and periods coincide in this limit. However, the time dependent phase shift is always present. One can say that this approximated solution $y(t,\lambda)$ is close to the exact solution $x(t)$ in the sense of orbital stability.

We propose to extend this approach to PDE systems. One should be mentioned that this approach is reminiscent of the modeling of micromorphic materials ([9], [21], [11], [12]) when it

is restricted to reversible processes. The formulation of the augmented lagrangian as a function of usual macroscopic and new dual variables is a rather intuitive procedure because the choice of the lagrangian is not unique. Also, some obvious constraints should be satisfied when such a lagrangian is constructed. Indeed,

- At least a one-parameter family of 'augmented' lagrangians should be properly choosen, giving in some limit (for example, when the parameter goes to infinity) the 'master' lagrangian.
- The Euler-Lagrange equations for the 'augmented' lagrangian should be unconditionally hyperbolic. It means that the corresponding Cauchy problem is well posed. If the equations are only conditionally hyperbolic, additional numerical problems can appear.
- In the linear approximation, the Whitham type condition [32] should be satisfied : the phase velocities of waves corresponding to the 'master ' lagrangian should be interplaced between the phase velocities corresponding to the 'augmented' lagrangian for any wave numbers. This condition is well known in hyperbolic equations where it is often called 'subcharacteristic' condition. In particular, it implies the linear stability of equilibrium solutions. Such a condition should also be satisfied for dispersive equations. In particular, it allows us to split the propagation wave modes and understand which one is responsible for the dispersive properties of the limit system.

In Section 2, the SGN equations as well as the corresponding 'master' lagrangian are presented. An 'augmented' lagrangian and the corresponding Euler-Lagrange equations are formulated in Section 3. A numerical method and numerical results are given in Sections 4 and 5. Technical details as well as a 2D extention of the model are presented in Appendices A, B and C.

2 The SGN equations

Consider the one-dimensional SGN equations describing dispersive non-linear long water waves in a one layer flow over a flat bottom. The dissipative effects are neglected. Under these assumptions the equations read :

$$\begin{aligned} &\frac{\partial h}{\partial t} + \frac{\partial hu}{\partial x} = 0, \\ &\frac{\partial hu}{\partial t} + \frac{\partial hu^2 + p}{\partial x} = 0, \text{ with } p = \frac{gh^2}{2} + \frac{1}{3}h^2\ddot{h}. \end{aligned} \tag{3}$$

Here $h > 0$ is the water depth, and u is the average horizontal velocity. The 'dot' means the material derivatives:

$$\dot{h} = \frac{\partial h}{\partial t} + u\frac{\partial h}{\partial x}, \quad \ddot{h} = \left(\frac{\partial}{\partial t} + u\frac{\partial}{\partial x}\right)\dot{h}. \tag{4}$$

The system (3) admits a variational formulation with the master lagrangian (see [30], [13], [14], [15]) :

$$\mathcal{L} = \int_{-\infty}^{\infty} \left(\frac{hu^2}{2} - W(h, \dot{h})\right) dx, \tag{5}$$

where the potential $W(h, \dot{h})$ is :

$$W(h, \dot{h}) = \frac{gh^2}{2} - \frac{h\dot{h}^2}{6}. \tag{6}$$

To simplify the derivation of the governing equations, we will use the mass Lagrangian coordinate q instead of the Eulerian coordinate x :

$$q = \int_0^X h_0(s)ds,$$

where X is the classical Lagrangian coordinate, and $h_0(X)$ is the initial data for the fluid depth. Let $\tau = \dfrac{1}{h}$. The lagrangian reads then:

$$\mathcal{L} = \int_{-\infty}^{\infty} L\, dq, \quad L = \frac{u^2}{2} - \tilde{W}(\tau, \tau_t), \tag{7}$$

with

$$u = x_t, \quad \tau = x_q, \quad \tilde{W}(\tau, \tau_t) = \frac{g}{2\tau} - \frac{1}{6}\left(\frac{\partial 1/\tau}{\partial t}\right)^2.$$

The governing equations in (t, q) variables can be written as :

$$\tau_t - u_q = 0, \quad u_t + p_q = 0, \tag{8}$$

with

$$p = -\frac{\delta \tilde{W}}{\delta \tau} = -\left(\frac{\partial \tilde{W}}{\partial \tau} - \frac{\partial}{\partial t}\left(\frac{\partial \tilde{W}}{\partial \tau_t}\right)\right) = \frac{g}{2\tau^2} + \frac{2}{3}\frac{\tau_t^2}{\tau^5} - \frac{1}{3}\frac{\tau_{tt}}{\tau^4}. \tag{9}$$

They admit the energy conservation law :

$$\left(\frac{u^2}{2} + e\right)_t + (pu)_q = 0,$$

with

$$e = \frac{g}{2\tau} + \frac{1}{6}\frac{\tau_t^2}{\tau^4}.$$

3 The method of an 'augmented' lagrangian for the SGN equations

Let $\tau = x_q$, and $u = x_t$. We take the augmented lagrangian under the following form :

$$\hat{\mathcal{L}} = \int_{-\infty}^{\infty} \hat{L}\, dq, \quad \hat{L} = \frac{x_t^2}{2} + \frac{\eta_t^2}{6} - \frac{g}{2\tau} - \alpha(\tau, \eta)\frac{(\eta - \frac{1}{\tau})^2}{6}. \tag{10}$$

We introduced here a non-equilibrium variable η having the propriety that in equilibrium, one has $\eta = \frac{1}{\tau}$. To guarantee the convergence (weak) of the solutions of the Euler-Lagrange equations for the lagrangian (10), to the solutions of the SGN equations (8)-(9), the function $\alpha(\tau, \eta)$ should be quite large. Below, we will precise this function. Let us consider the following three one-parameter families of lagrangians corresponding to different choices of $\alpha(\tau, \eta)$:

$$\hat{\mathcal{L}} = \int_{-\infty}^{\infty} \hat{L}\, dq, \quad \hat{L} = \frac{x_t^2}{2} + \frac{\eta_t^2}{6} - \frac{g}{2\tau} - \lambda\frac{(\eta - \frac{1}{\tau})^2}{6}, \quad \alpha = \lambda = const > 0. \tag{11}$$

$$\hat{\mathcal{L}} = \int_{-\infty}^{\infty} \hat{L}\, dq, \quad \hat{L} = \frac{x_t^2}{2} + \frac{\eta_t^2}{6} - \frac{g}{2\tau} - \lambda\frac{(\eta\tau - 1)^2}{6}, \quad \alpha = \lambda\tau^2, \quad \lambda = const > 0. \tag{12}$$

$$\hat{\mathcal{L}} = \int_{-\infty}^{\infty} \hat{L}\, dq, \quad \hat{L} = \frac{x_t^2}{2} + \frac{\eta_t^2}{6} - \frac{g}{2\tau} - \lambda \frac{(\eta\tau - 1)^4}{6}, \quad \alpha = \lambda\tau^2(\eta\tau - 1)^2, \quad \lambda = const > 0. \quad (13)$$

In every case (11) - (13), the parameter $\lambda > 0$ is large. It plays the role of penalty coefficient : when it tends to infinity, $\eta\tau - 1$ vanishes, and all lagrangians converge to the master lagrangian (7). The multiplier $1/6$ is introduced for convenience. In the following, we will highlight the properties of each lagrangian. In particular, we will show that only lagrangian (12) is mathematically satisfactory, the other lagrangians have some defaults. The properties of the lagrangian (12) are detailed in Section 3.2.

3.1 First lagrangian

We consider first the extended lagrangian (11). The corresponding Euler-Lagrange equations read :

$$\begin{cases} -\dfrac{\partial}{\partial t}\left(\dfrac{\partial \hat{L}}{\partial x_t}\right) - \dfrac{\partial}{\partial q}\left(\dfrac{\partial \hat{L}}{\partial x_q}\right) = 0, \\ \dfrac{\partial \hat{L}}{\partial \eta} - \dfrac{\partial}{\partial t}\left(\dfrac{\partial \hat{L}}{\partial \eta_t}\right) = 0. \end{cases}$$

Complemented with the mass conservation law which is just the compatibility condition $\tau_t - u_q = 0$ with $\tau = x_q$ and $u = x_t$, they can be rewritten as :

$$\begin{cases} \tau_t - u_q = 0, \\ u_t - \left(\dfrac{g}{\tau^3} + \dfrac{\lambda}{\tau^3}\left(\dfrac{1}{\tau} - \dfrac{2}{3}\eta\right)\right)\tau_q - \dfrac{\lambda}{3}\dfrac{\eta_q}{\tau^2} = 0, \\ \eta_{tt} = \lambda\left(\dfrac{1}{\tau} - \eta\right). \end{cases}$$

This system can be rewritten in conservative form :

$$\begin{cases} \tau_t - u_q = 0, \\ u_t + \left(\dfrac{g}{2\tau^2} + \dfrac{\lambda}{3\tau^2}\left(\dfrac{1}{\tau} - \eta\right)\right)_q = 0, \\ \eta_t = w, \\ w_t = \lambda\left(\dfrac{1}{\tau} - \eta\right). \end{cases} \quad (14)$$

The characteristic slopes are :

$$\xi_{1,2} = 0, \quad \xi_{3,4} = \pm\sqrt{\frac{g}{\tau^3} + \frac{\lambda}{\tau^3}\left(\frac{1}{\tau} - \frac{2}{3}\eta\right)}.$$

This model is hyperbolic if $\eta < \dfrac{3}{2}\left(\dfrac{g}{\lambda} + \dfrac{1}{\tau}\right)$. This system is similar to the one proposed by Liapidevskii and Gavrilova (2008) [23] where a different approach based on the averaging of instantaneous variables was used. Due to the Noether theorem, system (14) admits the energy conservation law :

$$\left(\frac{u^2}{2} + \frac{w^2}{6} + \frac{g}{2\tau} + \lambda\frac{(\eta\tau - 1)^2}{6\tau^2}\right)_t + (pu)_q = 0, \quad p = \frac{g}{2\tau^2} + \frac{\lambda}{3\tau^2}\left(\frac{1}{\tau} - \eta\right).$$

The system (14) is only conditionally hyperbolic, so it does not satisfy all the constraints mentioned in the Introduction.

3.2 Second lagrangian

Consider now the extended lagrangian (12). The Euler-Lagrange equations are :

$$\begin{cases} u_t - \left(\frac{g}{\tau^3} + \frac{\lambda}{3}\eta^2\right)\tau_q - \frac{\lambda}{3}(2\tau\eta - 1)\eta_q = 0, \\ \eta_{tt} = -\lambda\left(\eta\tau - 1\right)\tau. \end{cases} \tag{15}$$

This system can be rewritten in conservative form :

$$\begin{cases} \tau_t - u_q = 0, \\ u_t + \left(\frac{g}{2\tau^2} - \frac{\lambda}{3}(\tau\eta - 1)\eta\right)_q = 0, \\ \eta_t = w, \\ w_t = -\lambda\left(\eta\tau - 1\right)\tau. \end{cases} \tag{16}$$

This system is unconditionally hyperbolic, the characteristic slopes are :

$$\xi_{1,2} = 0, \quad \xi_{3,4} = \pm\sqrt{\frac{g}{\tau^3} + \frac{\lambda}{3}\eta^2} \tag{17}$$

The eigenfields corresponding to $\xi_{1,2}$ ($\xi_{3,4}$) are linearly degenerate (genuinely nonlinear in the sense of Lax). The proof is given in Appendix B. System (16) admits the energy conservation law :

$$\left(\frac{u^2}{2} + \frac{w^2}{6} + \frac{g}{2\tau} + \lambda\frac{(\eta\tau - 1)^2}{6}\right)_t + (pu)_q = 0, \quad p = \frac{g}{2\tau^2} - \frac{\lambda}{3}\left(\tau\eta - 1\right)\eta.$$

For the original Green-Naghdi model (8) - (9) linearised at $u = 0, \tau = \tau_0$ the phase velocity $c_p = \omega/k$ is :

$$c_p^2 = \frac{g}{\tau_0^3 + \frac{k^2}{3\tau_0}} \tag{18}$$

For the new model, the phase velocity reads (see Appendix A for details):

$$\left(c_p^{\pm}\right)^2 = \frac{\frac{g}{\tau_0^3} + \frac{\lambda}{3\tau_0^2} + \frac{\lambda\tau_0^2}{k^2} \pm \sqrt{\left(\frac{g}{\tau_0^3} + \frac{\lambda}{3\tau_0^2} + \frac{\lambda\tau_0^2}{k^2}\right)^2 - 4\frac{g\lambda}{\tau_0 k^2}}}{2}. \tag{19}$$

The phase velocity corresponding to the sign 'minus' ('plus') is called *slow* (*rapid*) phase velocity. The phase velocity c_p corresponding to the master lagrangian is interplaced between the phase velocities corresponding to augmented lagrangian for any wave number k (see Figures 1 and 2), so the Whitham type condition is also satisfied :

$$-c_p^+(\lambda) < -c_p < -c_p^-(\lambda) < 0 < c_p^-(\lambda) < c_p < c_p^+(\lambda).$$

It follows from (18) that

$$\left(c_p^-\right)^2 = \frac{g}{\tau_0^3 + \frac{k^2}{3\tau_0}} + \frac{g}{\lambda}\frac{g^2k^4}{(k^2 + 3\tau_0^4)^3} + \mathcal{O}\left(\frac{1}{\lambda^2}\right), \ \left(c_p^+\right)^2 = \mathcal{O}\left(\lambda\right),$$

so $c_p^-(\lambda) \to c_p$ as $\lambda \to \infty$ (see also Figure 1).

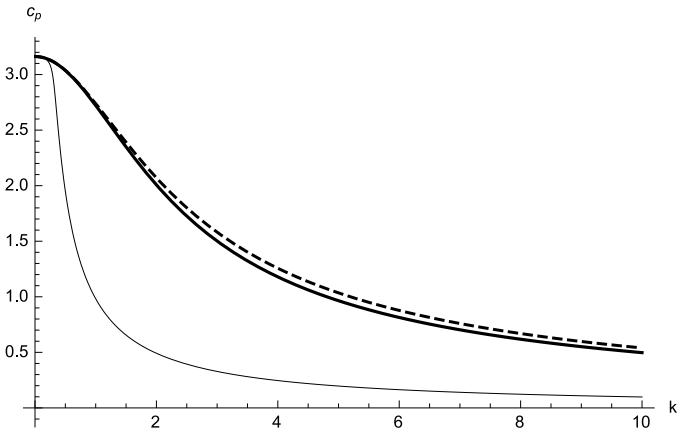

Figure 1: The slow phase velocity c_p^- defined by (19) is shown as a function of the wave number k for $\lambda = 1\ m^2/s^2$ (thin line) and $\lambda = 160\ m^2/s^2$ (thick line). The value of τ_0 is $1\ m^{-1}$. When the parameter λ is sufficiently large, the phase velocity is close to that of the SGN model defined by (18) (dashed line).

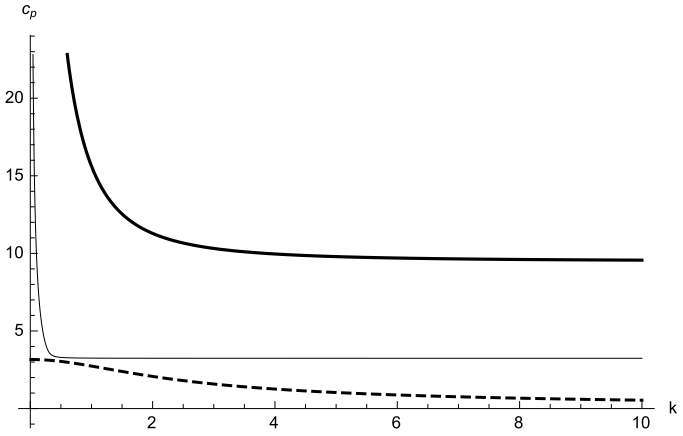

Figure 2: The rapid phase velocity c_p^+ is shown as a function of the wave number k for the new model with $\lambda = 1\ m^2/s^2$ (thin line) and $\lambda = 160\ m^2/s^2$ (thick line). The value of τ_0 is $1\ m^{-1}$. The velocity c_p^+ is always higher then that of the SGN model (dashed line). It describes the evolution of 'parasitic' high-frequency waves related to the modification of the lagrangian.

3.3 Third lagrangian

Let us consider now the extended lagrangian (13). The Euler-Lagrange equations are :

$$\begin{cases} u_t - \left(\frac{g}{\tau^3} + 2\lambda(\eta\tau - 1)^2\eta^2\right)\tau_q - \frac{2\lambda}{3}(\tau\eta - 1)^2(4\tau\eta - 1)\eta_q = 0, \\ \eta_{tt} = -2\lambda\left(\eta\tau - 1\right)^3\tau. \end{cases}$$

Again, this system can be rewritten in conservative form :

$$\begin{cases} \tau_t - u_q = 0, \\ u_t + \left(\frac{g}{2\tau^2} - \frac{2\lambda}{3}(\tau\eta - 1)^3\eta\right)_q = 0, \\ \eta_t = w, \\ w_t = -2\lambda\left(\eta\tau - 1\right)^3\tau. \end{cases} \tag{20}$$

This system is unconditionally hyperbolic, with the following characteristic slopes :

$$\xi_{1,2} = 0, \quad \xi_{3,4} = \pm\sqrt{\frac{g}{\tau^3} + 2\lambda(\eta\tau - 1)^2\eta^2}.$$

System (20) admits the energy conservation law :

$$\left(\frac{u^2}{2} + \frac{w^2}{6} + \frac{g}{2\tau} + \lambda\frac{(\eta\tau - 1)^4}{6}\right)_t + (pu)_q = 0, \quad p = \frac{g}{2\tau^2} - \frac{2\lambda}{3}\left(\tau\eta - 1\right)^3\eta.$$

The phase velocity of linear waves does not depend on the wave number :

$$c_p^2 = \frac{g}{\tau^3}.$$

Since the dispersion effects are not captured in the linear approximation, the model is not able to deal with accurate description of the SGN equations.

In the following, we will concentrate on the numerics of the Euler-Lagrange equations (16) obtained from the second lagrangian (12).

4 Numerical resolution

The lagrangian form of system (16) is :

$$\frac{\partial\tilde{\mathbf{U}}}{\partial t} + \frac{\partial\tilde{\mathbf{F}}}{\partial q} = \tilde{\mathbf{S}},$$

with $\tilde{\mathbf{U}} = (\tau, u, \eta, w)^T$, $\tilde{\mathbf{F}} = \left(-u, \frac{g}{2\tau^2} - \frac{\lambda}{3}(\tau\eta - 1)\eta, 0, 0\right)^T$ and $\tilde{\mathbf{S}} = (0, 0, w, -\lambda\tau(\eta\tau - 1))^T$. The Eulerian form of system (16) is :

$$\frac{\partial\mathbf{U}}{\partial t} + \frac{\partial\mathbf{F}}{\partial x} = \mathbf{S}, \tag{21}$$

with $\mathbf{U} = (h, hu, h\eta, hw)^T$, $\mathbf{F} = \left(hu, hu^2 + \frac{gh^2}{2} - \frac{\lambda}{3}(\frac{\eta}{h} - 1)\eta, h\eta u, hwu\right)^T$ and $\mathbf{S} = \left(0, 0, hw, -\lambda(\frac{\eta}{h} - 1)\right)^T$. In the following, we will use the Eulerian form (21) to have a possibility to compare the numerical results with other numerical approaches. The structure of the eigenfields is analysed in the Appendix B. For completeness, we also present in Appendix C the multi-dimensional version of

(21). Since, the system is hyperbolic and conservative, a classical Godunov - type method can be used followed by the Strang splitting strategy. Equations (21) are split into a hyperbolic part :

$$\frac{\partial \mathbf{U}}{\partial t} + \frac{\partial \mathbf{F}}{\partial x} = 0, \tag{22}$$

and an ODE part (the treatment of the right-hand side $\mathbf{S}$):

$$\frac{\partial \mathbf{U}}{\partial t} = \mathbf{S}. \tag{23}$$

The operators associated with the discretization of (22) and (23) are denoted $\mathbf{H}_h$ and $\mathbf{H}_r$, respectively. The second-order Strang splitting procedure is used, solving successively (22) and (23) with adequate time increments:

$$\begin{cases} \mathbf{U}_i^{(1)} = \mathbf{H}_r\left(\dfrac{\Delta t}{2}\right)\mathbf{U}_i^n, \\ \mathbf{U}_i^{(2)} = \mathbf{H}_h\left(\Delta t\right)\mathbf{U}_i^{(1)}, \\ \mathbf{U}_i^{n+1} = \mathbf{H}_r\left(\dfrac{\Delta t}{2}\right)\mathbf{U}_i^{(2)}. \end{cases} \tag{24}$$

Since $\mathbf{H}_h$ and $\mathbf{H}_r$ are of second order accuracy operators, the procedure (24) gives us a second-order accuracy approximation of (21) [24].

4.1 Hyperbolic step

The equation (22) is solved by a conservative scheme for hyperbolic systems [24]

$$\mathbf{U}_i^{n+1} = \mathbf{U}_i^n - \frac{\Delta t}{\Delta x}\left(\mathbf{F}_{i+1/2}^* - \mathbf{F}_{i-1/2}^*\right) \tag{25}$$

The numerical flux function $\mathbf{F}_{i+1/2}^*$ is computed here by using the Rusanov method [28]:

$$\mathbf{F}_{i+1/2}^* = \frac{1}{2}\left(\mathbf{F}(\mathbf{U}_{i+1}^n) + \mathbf{F}(\mathbf{U}_i^n) - \kappa_{i+1/2}^n(\mathbf{U}_{i+1}^n - \mathbf{U}_i^n)\right). \tag{26}$$

The parameter $\kappa_{i+1/2}^n$ is obtained by using the Davis approximation [6] :

$$\kappa_{i+1/2}^n = \max_j(|c_j(\mathbf{U}_i^n)|, |c_j(\mathbf{U}_{i+1}^n)|), \tag{27}$$

where c_j are the eigenvalues of (21). The usual Courant-Friedrichs-Lewy (CFL) condition is satisfied :

$$\Delta t = CFL\frac{\Delta x}{|c_{max}|}, \text{ with } CFL < 1, \tag{28}$$

where c_{max} is the maximal value of the characteristic velocities over the mesh. Any other reasonable Riemann solver can also be used at this step.

4.2 ODE step

The source terms treatment is reduced to a second order ordinary differential equation with constant coefficients which can be solved exactly. Indeed, for system (16), the relaxation system

(23) is :

$$\begin{array}{l} \dfrac{\partial u}{\partial t} = 0, \\ \dfrac{\partial \tau}{\partial t} = 0, \\ \dfrac{\partial \eta}{\partial t} = w, \\ \dfrac{\partial w}{\partial t} = \lambda \left(1 - \eta\tau\right) \tau. \end{array} \tag{29}$$

It comes :

$$\begin{array}{c} u(t+\Delta t) = u(t), \quad \tau(t+\Delta t) = \tau(t), \\ \eta(t+\Delta t) = \left(\eta(t) - \dfrac{1}{\tau(t)}\right) \cos\left(\tau(t)\sqrt{\lambda}\Delta t\right) + \dfrac{w(t)}{\tau(t)\sqrt{\lambda}} \sin\left(\tau(t)\sqrt{\lambda}\Delta t\right) + \dfrac{1}{\tau(t)}, \\ w(t+\Delta t) = \left(-\tau(t)\sqrt{\lambda}\left(\eta(t) - \dfrac{1}{\tau(t)}\right) \sin\left(\tau(t)\sqrt{\lambda}\Delta t\right) + w(t)\cos\left(\tau(t)\sqrt{\lambda}\Delta t\right)\right). \end{array} \tag{30}$$

5 Numerical results

5.1 Solitary wave solutions

Solitary wave solutions to the SGN system depending on $\xi = x - Dt$, D is a constant wave velocity, are :

$$\begin{array}{l} h(\xi) = h_1 + (h_2 - h_1)\mathrm{sech}^2\left(\frac{\xi}{2}\sqrt{\frac{3(h_2-h_1)}{h_2 h_1^2}}\right), \\ u(\xi) = D\left(1 - \frac{h_1}{h(\xi)}\right), \ D^2 = g h_2. \end{array} \tag{31}$$

In the following example, we take $h_1 = 1\ m$, $h_2 = 1.8\ m$ and $g = 10\ m/s^2$. We initialise the density and the velocity with the exact solution and we impose $\eta = h$ and $w = 0$. The maximum of the solitary wave, moving to the right, was initially situated at $x = 200\ m$. One can notice that the initial data is not an exact solution to the extended system (21). Indeed, the pressure in the SGN system given by $p = \frac{1}{2}gh^2 + \frac{1}{3}h^2\ddot{h}$ is not initially hydrostatic, while it is the case in the augmented system. Then, the solution to the augmented system evolves. We represent the results for different mesh sizes at different time instants on Figure 3 (for $\lambda = 300\ m^2/s^2$) and Figure 4 (for $\lambda = 1200\ m^2/s^2$). On these Figures, one can observe small amplitude perturbations due to the error in the initial conditions. On Figure 5, we represent at time instant $t = 160\ s$ the exact solution (31) of the SGN equations (dashed line), solution of (21) for $\lambda = 300\ m^2/s^2$ (thin line) and $\lambda = 1200\ m^2/s^2$ (thick line). The shape and amplitude of solitary waves are good for both cases. As it was discussed in the introduction, the phase shift depending on λ can not be controlled.

On Figure 6, we represent the evolution of the error in determining the amplitude of solitary wave as a function of the mesh size for different values of λ. The numerical results converge. One can note that for a coarser mesh, one should use a smaller value of λ. When the mesh cell size decreases, a larger value of λ will give more precise results. In practice, we choose first the value of λ approaching the dispersion relation with a given accuracy, and then we refine the mesh.

5.2 Favre waves

We consider the experiment where a fluid layer with a free surface is impacting a wall ('water hammer problem with a free surface') [10], [31]. Due to dispersion, the reflected wave is rather a wave train of waves of different lengths and amplitudes (called also 'Favre waves', see Figure

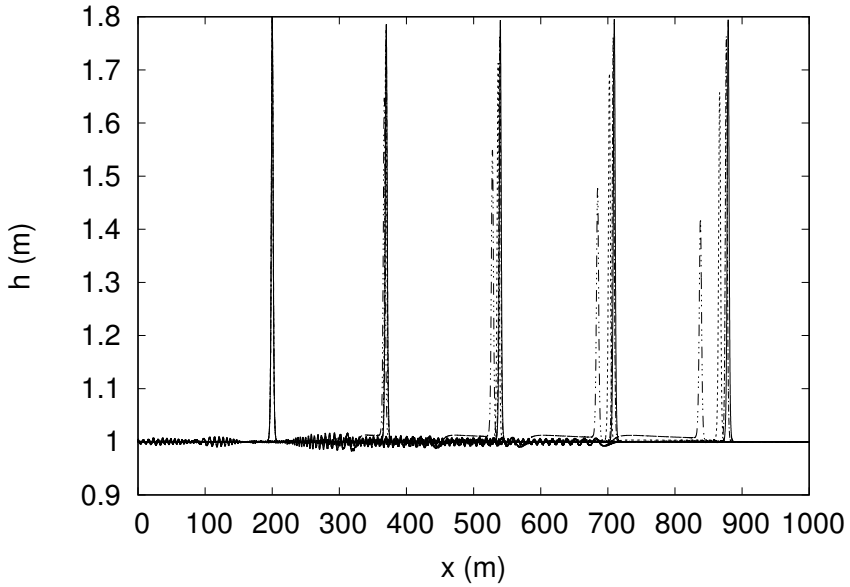

Figure 3: Evolution of the solitary wave initially situated at $x = 200\ m$ and moving to the right, is shown at time instants $t = 40\ s$, $t = 80\ s$, $t = 120\ s$ and $t = 160\ s$ with $\lambda = 300\ m^2/s^2$ for different mesh sizes : $\Delta x = 0.1\ m$ (dash-triple-dotted lines), $\Delta x = 5\ cm$ (dashed lines), $\Delta x = 2.5\ cm$ (dash-dotted lines) and $\delta x = 1.25\ cm$ (continuous lines). The second order extension with Minmod limiter with $CFL = 0.5$ is used here.

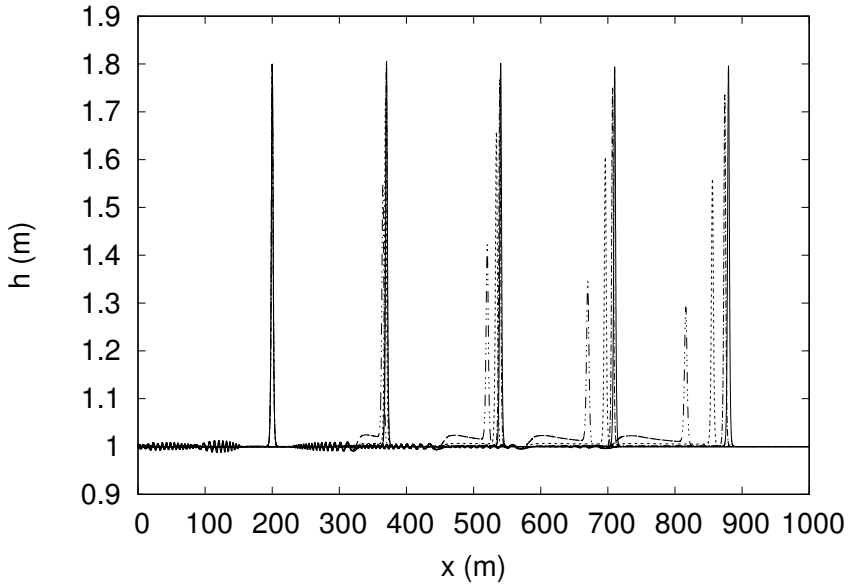

Figure 4: Evolution of the solitary wave initially situated at $x = 200\ m$ and moving to the right, is shown at time instants $t = 40\ s$, $t = 80\ s$, $t = 120\ s$ and $t = 160\ s$ with $\lambda = 1200\ m^2/s^2$ for different mesh sizes : $\Delta x = 0.1\ m$ (dash-triple-dotted lines), $\Delta x = 5\ cm$ (dashed lines), $\Delta x = 2.5\ cm$ (dash-dotted lines) and $\delta x = 1.25\ cm$ (continuous lines). The second order extension with Minmod limiter with $CFL = 0.5$ is used here.

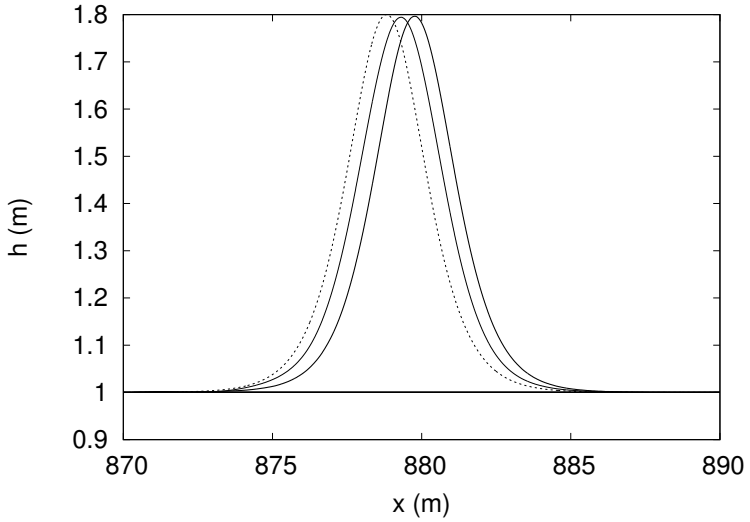

Figure 5: Comparison of the solution at time $t = 160\ s$ for 80000 mesh cells at 1000 m ($\Delta x = 1.25\ cm$). The exact solution is represented with dashed line. The solution with $\lambda = 300\ m^2/s^2$ ($\lambda = 1200\ m^2/s^2$) is represented with thin (thick) lines. The agreement on the shape is very good. There is a small shift in the position of the solitary wave.

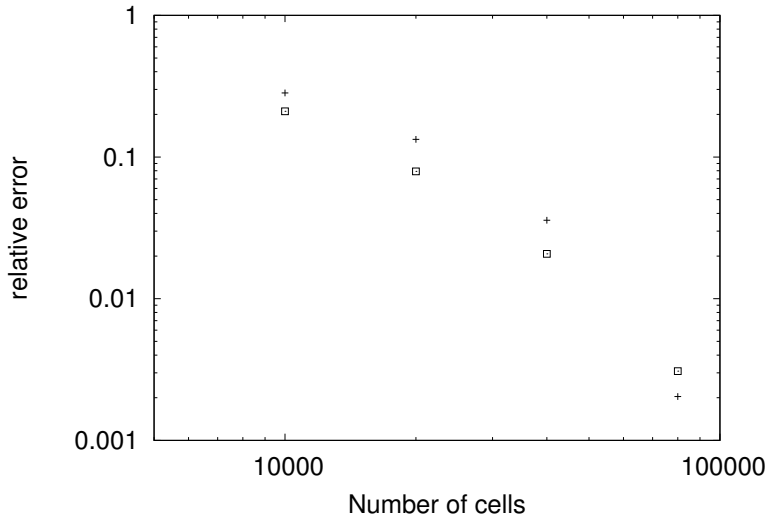

Figure 6: Relative error on the amplitude of the solitary wave. The results with $\lambda = 300\ m^2/s^2$ (respectively $\lambda = 1200\ m^2/s^2$) are represented with squares (respectively with crosses). One can observe that on a coarse mesh, the numerical dissipation is the main source of error, because the numerical viscosity is proportional to the characteristic velocity. For a thinner mesh, the results obtained with larger values of λ are better.

7). The SGN equations can be used to model this problem until some critical impact velocity determined in terms of the relative (with respect to the velocity of the reflected wave) Froude number F. Above this critical value, the model is not valid because of the wave breaking (see [16] for details). To avoid the difficulties related to the wall boundary conditions, we consider a symmetric impact test problem. The impact velocity u_0 is related to the relative Froude number F by the formula [16] :

$$u_0 = \sqrt{gh_0}\left(F - \frac{1+\sqrt{1+8F^2}}{4F}\right)$$

In Figure 8, we compare the numerical results at time $t = 54\ s$ with the results obtained by the method [20]. The continuous blue line corresponds to the numerical solution of the SGN equations obtained by the method [20] on a 32000 cell mesh. Our results (second order extension with Van Leer Limiter) were obtained on different meshes (2000, 4000 and 8000 cells) (see Figure 8). One can observe that the results for 4000 and 8000 cells are almost superposed. Thus, a good estimation of the first wave amplitude can be obtained with a coarser mesh. In Table 9, we show the computational time for the different mesh sizes. In Figure 10, we represent the evolution of the computational time with the mesh size (normalized with the computational time of the coarser grid). One can see that the computational time increases much slower with the mesh refinement for the new hyperbolic approach. Moreover, the new approach is well adapted for the parallelisation technique based on the domain decomposition methods. Indeed, the equations being hyperbolic, the 'interaction' between domains is always local. In Figure 11, the numerical results are compared with the experiments of [31]. The results are in perfect agreement with experiments until the wave breaking occurs corresponding to the Froude number about 1.25.

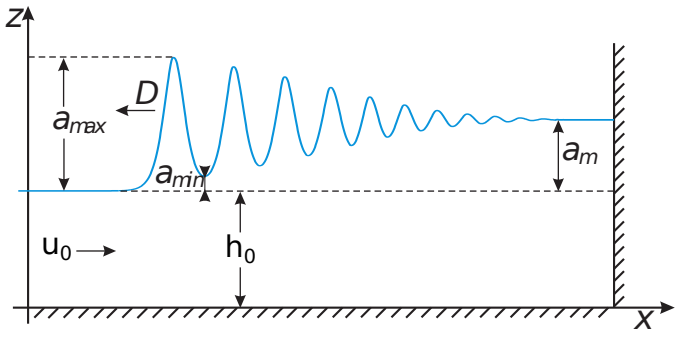

Figure 7: A sketch of Favre waves.

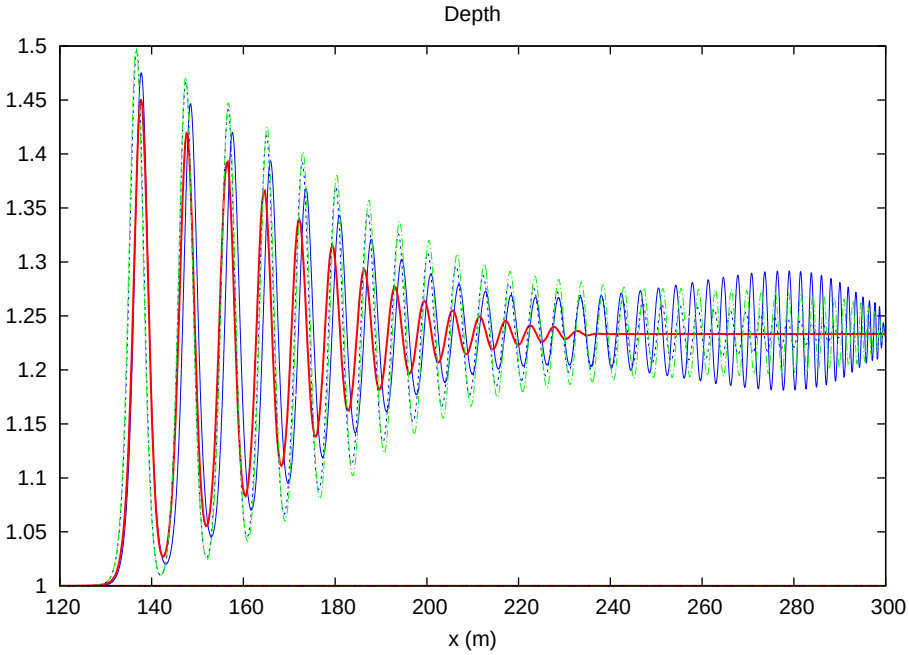

Figure 8: Comparison at time $t = 54\ s$ for the Froude number $Fr = 1.16$ in the Favre experiment. It corresponds to $h_0 = 1\ m$ and the impact velocity $u_0 = 0.2\sqrt{gh_0}\ m/s$, $g = 10\ m/s$. The result obtained by the method developed in [20] on a 32000 cell mesh is shown with a thin continuous blue line. The results obtained with the second order extension of the new model with $\lambda = 300$ are shown for different mesh sizes : 2000 (red thick continuous line), 4000 (blue dashed line), 8000 (green dash-dotted line). The agreement is good and the convergence is guaranteed.

Mesh size	Hyperbolic model	Approach [20]
2000	1.12	12.44
4000	4.65	191.84
8000	19.32	1844
16000	75.52	21200

Figure 9: Computational time (in seconds) for the hyperbolic model and for the approach [20].

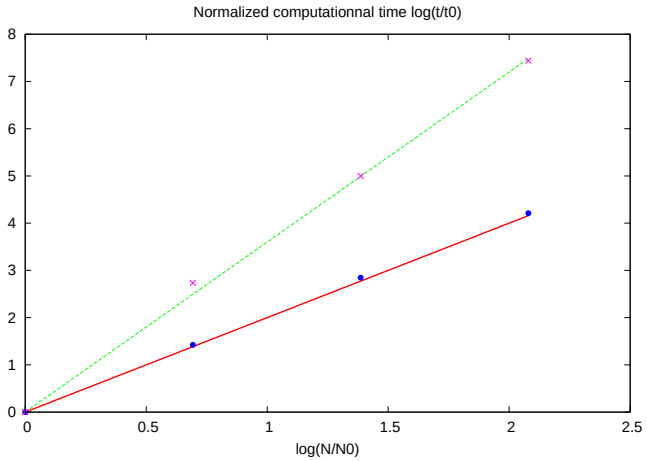

Figure 10: Computational time versus mesh size normalized by $N_0 = 2000$. The crosses correspond to the method [20], the dots correspond to the new hyperbolic method. The dashed line has the slope 3.6 while the continuous line has a slope 2. The computational time increases much faster for the approach [20].

6 Conclusion

A new numerical approach based on the notion of 'augmented' lagrangian is proposed to solve dispersive equations. The corresponding Euler-Lagrange equations are hyperbolic and approximate the Serre-Green-Naghdi equations with a good accuracy. The computational time with the new approach is much lower compared to the traditional methods. Thus, it is now possible to think about multi-dimensional resolution with a reasonable computational time. Higher order extension based on WENO, ADER or other methods can also be easily developed. The same approach can also be applied to modelling fluids containing gas bubbles, because the governing equations have the same mathematical structure [13], [14].

Acknowledgment This work has been partially supported by the ANR project Bond-ANR-13-BS01-0009-02, and by the Russian Science Foundation (grant No. 15-11-20013). The authors thank V. Yu. Liapidevskii, A. Madeo and P. Seppecher for helpful discussions, and anonymous reviewers for their careful reading of our manuscript and their many insightful comments and suggestions.

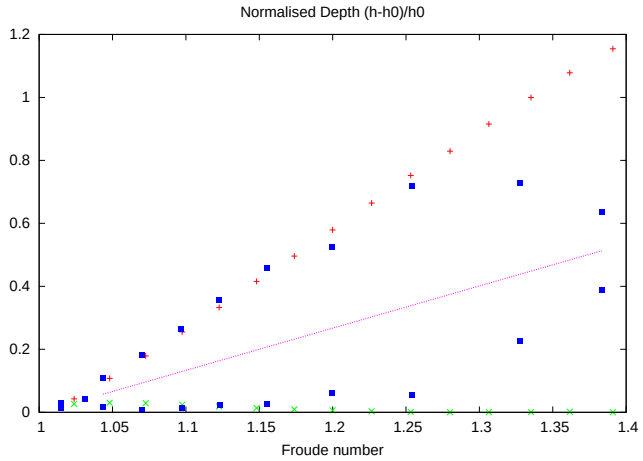

Figure 11: Comparison between the experimental results of [31] (squares) and the numerical results. The upper squares indicate the amplitude of the first wave, while the lower squares show the amplitude of the trough after the first wave. The agreement is perfect until the Froude number about 1.25. After this critical value, the model is no more valid, the wave breaking occurs which is not described by the SGN model (see [16] for modelling of breaking waves). The middle straight line corresponds to the solution of the Saint-Venant equations.

A Dispersion relation

We consider the Euler-Lagrange equations for (12) :

$$\left\{\begin{array}{l} \tau_t - u_q = 0, \\ u_t - \left(\dfrac{g}{\tau^3} + \dfrac{\lambda}{3}\eta^2\right)\tau_q - \dfrac{\lambda}{3}(2\tau\eta - 1)\eta_q = 0, \\ \eta_{tt} = -\lambda\left(\eta\tau - 1\right)\tau. \end{array}\right. \tag{32}$$

Consider the perturbation of a constant state $u = 0$, $\tau = \tau_0$, $\eta = \eta_0$, $\tau_0\eta_0 = 1$: $u = \varepsilon\tilde{u}$, $\tau = \tau_0 + \varepsilon\tilde{\tau}$, $\eta = \eta_0 + \varepsilon\tilde{\eta}$. At first order the system reads :

$$\left\{\begin{array}{l} \tilde{\tau}_t - \tilde{u}_q = 0, \\ \tilde{u}_t - \left(\dfrac{g}{\tau_0^3} + \dfrac{\lambda}{3}\eta_0^2\right)\tilde{\tau}_q - \dfrac{\lambda}{3}(2\tau_0\eta_0 - 1)\tilde{\eta}_q = 0, \\ \tilde{\eta}_{tt} = -\lambda\left(\tilde{\eta}\tau_0^2 + \tilde{\tau}\right). \end{array}\right.$$

We consider monochromatic perturbations : $\tilde{u} = u_1 e^{i(kx-\omega t)}$, $\tilde{\tau} = \tau_1 e^{i(kx-\omega t)}$ and $\tilde{\eta} = \eta_1 e^{i(kx-\omega t)}$. We get :

$$\left\{\begin{array}{l} \omega\tau_1 + ku_1 = 0, \\ \omega u_1 + \left(\dfrac{g}{\tau_0^3} + \dfrac{\lambda}{3\tau_0^2}\right)k\tau_1 + \dfrac{\lambda}{3}k\eta_1 = 0, \\ \omega^2\eta_1 - \lambda\left(\eta_1\tau_0^2 + \tau_1\right) = 0. \end{array}\right.$$

It can be also written as :

$$\mathbf{A}\mathbf{x} = 0, \quad \mathbf{x}^T = (\tau_1, u_1, \eta_1),$$

with

$$\mathbf{A} = \begin{pmatrix} \omega & k & 0 \\ k\left(\frac{g}{\tau_0^2} + \frac{\lambda}{3\tau_0^2}\right) & \omega & \frac{\lambda k}{3} \\ -\lambda & 0 & \omega^2 - \lambda\tau_0^2 \end{pmatrix}.$$

The corresponding homogeneous linear system has non-trivial solution if and only if the determinant of $\mathbf{A}$ is zero :

$$c_p^4 - c_p^2\left(\frac{g}{\tau_0^3} + \frac{\lambda}{3\tau_0^2} + \frac{\lambda\tau_0^2}{k^2}\right) + \frac{g\lambda}{\tau_0 k^2} = 0.$$

The equation has two real positive roots $\left(c_p^{\pm}\right)^2$:

$$\left(c_p^{\pm}\right)^2 = \frac{\frac{g}{\tau_0^3} + \frac{\lambda}{3\tau_0^2} + \frac{\lambda\tau_0^2}{k^2} \pm \sqrt{\left(\frac{g}{\tau_0^3} + \frac{\lambda}{3\tau_0^2} + \frac{\lambda\tau_0^2}{k^2}\right)^2 - 4\frac{g\lambda}{\tau_0 k^2}}}{2}. \tag{33}$$

B Structure of the eigenfields

Let us consider the hyperbolic part of the system (21) :

$$\frac{\partial \mathbf{U}}{\partial t} + \frac{\partial \mathbf{F}}{\partial x} = 0,$$

with $\mathbf{U} = (h, hu, h\eta, hw)^T$, $\mathbf{F} = \left(hu, hu^2 + \frac{gh^2}{2} - \frac{\lambda}{3}(\frac{\eta}{h} - 1)\eta, h\eta u, hwu\right)^T$. This system can be rewritten under the following form :

$$\frac{\partial \mathbf{W}}{\partial t} + \mathbf{A}(\mathbf{W})\frac{\partial \mathbf{W}}{\partial x} = 0$$

with $\mathbf{W} = (h, u, \eta, w)^T$ and

$$\mathbf{A} = \begin{pmatrix} u & h & 0 & 0 \\ g + \frac{\lambda\eta^2}{3h^3} & u & -\frac{1}{3}\lambda\left(\frac{2\eta}{h} - 1\right) & 0 \\ 0 & 0 & u & 0 \\ 0 & 0 & 0 & u \end{pmatrix}$$

The eigenvalues of $\mathbf{A}$ are :

$$c_{1,2} = u,\ c_3 = u - \sqrt{gh + \frac{\lambda}{3}\frac{\eta^2}{h^2}},\ c_4 = u + \sqrt{gh + \frac{\lambda}{3}\frac{\eta^2}{h^2}}.$$

The associate right eigenvectors are :

$$\mathbf{v}_1 = (0, 0, 0, 1)^T,$$

$$\mathbf{v}_2 = \left(\frac{\lambda}{3}\left(2\frac{\eta}{h} - 1\right), 0, g + \frac{\lambda}{3}\frac{\eta^2}{h^3}, 0\right)^T,$$

$$\mathbf{v}_3 = \left(-h, \sqrt{gh + \frac{\lambda}{3}\frac{\eta^2}{h^2}}, 0, 0\right)^T,$$

$$\mathbf{v}_4 = \left(h, \sqrt{gh + \frac{\lambda}{3}\frac{\eta^2}{h^2}}, 0, 0\right)^T.$$

The field associated to the eigenvalues $c_{1,2}$ are linearly degenerate : $\nabla c_{1,2} \cdot \mathbf{v}_{1,2} = 0$. The field associated to the eigenvalues $c_{3,4}$ are genuinely non-linear in the sense of Lax :

$$\nabla c_{3,4} \cdot \mathbf{v}_{3,4} = \frac{3}{2} \frac{gh}{\sqrt{gh + \frac{\lambda}{3}\frac{\eta^2}{h^2}}} > 0.$$

C Multi-dimensional augmented lagrangian

The multi-dimensional generalisation of the lagrangian (12) in Eulerian coordinates is :

$$\hat{L} = \frac{h|\mathbf{u}|^2}{2} + \frac{h\dot{\eta}^2}{6} - \frac{gh^2}{2} - \frac{\lambda h}{6}\left(\frac{\eta}{h} - 1\right)^2.$$

The corresponding governing equations generalising (21) can easily be obtained following [15] :

$$h_t + \operatorname{div}(h\mathbf{u}) = 0,$$

$$(h\mathbf{u})_t + \operatorname{div}(h\mathbf{u} \otimes \mathbf{u} + pI) = 0,\ p = \frac{gh^2}{2} - \frac{\lambda\eta}{3}\left(\frac{\eta}{h} - 1\right),$$

$$\dot{\eta} = w,\ \dot{w} = -\frac{\lambda}{h}\left(\frac{\eta}{h} - 1\right),\ \dot{} = \frac{\partial}{\partial t} + \mathbf{u} \cdot \nabla,$$

where I is the identity tensor, $\otimes$ means the tensor product.

The equations admit the energy conservation law :

$$\left(h\left(\frac{|\mathbf{u}|^2}{2} + \frac{\dot{\eta}^2}{6} + \frac{gh}{2} + \frac{\lambda}{6}\left(\frac{\eta}{h} - 1\right)^2\right)\right)_t + \operatorname{div}\left(h\mathbf{u}\left(\frac{|\mathbf{u}|^2}{2} + \frac{\dot{\eta}^2}{6} + \frac{gh}{2} + \frac{\lambda}{6}\left(\frac{\eta}{h} - 1\right)^2\right) + p\mathbf{u}\right) = 0.$$

References

[1] Berdichevskii, V. L. Variational Principles of Continuum Mechanics, Springer Verlag, 2009.

[2] Benzoni-Gavage, S., Noble, P. & Rodrigues, L. M. (2014) Slow modulations of periodic waves in Hamiltonian PDEs, with applications to capillary fluids, J. Nonlinear Science, **24**, N 4, 711-768.

[3] Besse, C., Ehrhardt, M. & Lacroix-Violet (2016) Discrete Artificial Boundary Conditions for the Korteweg-de Vries Equation, Numer. Meth. for PDEs, **33**, 5, p. 1455 - 1484.

[4] Besse, C., Mésognon-Gireauy, B. & Noble, P. (2016) Artificial boundary conditions for the linearized Benjamin-Bona-Mahony equation https://hal.archives-ouvertes.fr/hal-01305360/document.

[5] Cattaneo, C. (1958) Sur une forme d'équation de la chaleur éliminant le paradoxe d'une propagation instantanée, Comptes Rendus de l'Académie des Sciences, **247**, 431–433.

[6] Davis, S. F. (1988) Simplified second-order Godunov-type methods. SIAM Journal on Scientific and Statistical Computing, 9(3), 445-473.

[7] Dumbser, M., Peshkov, I., Romenski, E. & Zanotti, O. (2016) High order ADER schemes for a unified first order hyperbolic formulation of continuum mechanics : viscous heat - conducting fluids and elastic solids, J. Comp. Physics, **314**, 824-862.

[8] El, G. A. & Hoefer, M. (2016) Dispersive shock waves and modulation theory, Physica D, **333**, 11-65.

[9] Eringen, A. C. Microcontinuum Field Theories, I: Foundation and Solids, Springer Verlag, 1999.

[10] Favre, H. 1935 Ondes de translation dans les canaux découverts. Dunod (Paris).

[11] Forest, S. (2009) Micromorphic approach for gradient elasticity, viscoplasticity and damage, **135**, 117-131.

[12] Forest, S. (2016) Nonlinear regularisation operators as derived from the micromorphic approach to gradient elasticity, viscoplasticity and domage. Proc. Royal Soc. A **472** : 20150755.

[13] Gavrilyuk, S. L. (1994) Large amplitude oscillations and their "thermodynamics" for continua with "memory", European J. Mechanics, B/Fluids, **13**, N 6, 753-764.

[14] Gavrilyuk, S. L. & Teshukov, V. M. (2001) Generalized vorticity for bubbly liquid and dispersive shallow water equations, Continuum Mechanics and Thermodynamics **13**, 365 - 382.

[15] Gavrilyuk, S. (2011) Multiphase Flow Modeling via Hamilton's principle. In the book : Variational Models and Methods in Solid and Fluid Mechanics, CISM Courses and Lectures, v. 535 (Eds. F. dell'Isola and S. Gavrilyuk), Springer, 2011.

[16] Gavrilyuk, S. L., Liapidevskii, V. Yu. & Chesnokov, A. A. (2016) Spilling breakers in shallow water : applications to Favre waves and to the shoaling and breaking of solitary waves, J. Fluid Mechanics, **808**, 441 - 468.

[17] Green, A. E., Laws, N. & Naghdi, P. M. (1974) On the theory of water waves. Proc. R. Soc. Lond. A, **338**, 4355.

[18] Green, A. E. & Naghdi, P. M. (1976) A derivation of equations for wave propagation in water of variable depth. J. Fluid. Mechanics, **78**, 237-246.

[19] Hedstrom, G. W. (1979) Nonreflecting Boundary Conditions for Nonlinear Hyperbolic Systems, J. Comp. Physics, **30**, 222-237.

[20] Le Métayer, O., Gavrilyuk, S., & Hank, S. (2010). A numerical scheme for the Green –Naghdi model. Journal of Computational Physics, 229(6), 2034-2045.

[21] Neff, P., Ghiba, I. D., Madeo, A., Placidi, L., and Rosi, G. (2014). A unifying perspective: the relaxed linear micromorphic continuum. Continuum Mechanics and Thermodynamics, 26(5), 639-681.

[22] Lannes, D. & Marche, F. (2015) A new class of fully nonlinear and weakly dispersive Green-Naghdi models for efficient 2D simulations, J. Comp. Physics, **282**, 238 - 268.

[23] Liapidevskii, V. Y., and Gavrilova, K. N. (2008). Dispersion and blockage effects in the flow over a sill. Journal of Applied Mechanics and Technical Physics, 49(1), 34-45.

[24] LeVeque, R. J. (2002) Finite volume methods for hyperbolic problems (Vol. 31). Cambridge university press.

[25] Montecinos, G. I., Lopez-Rios, J. C., Lecaros, R., Ortega, J. H. & Toro, E. F. (2016) An ADER-type scheme for a class of equations arising from the water-wave theory, Computers and Fluids **132** 76-93.

[26] Peshkov, I. & Romenski, E. (2016) A hyperbolic model for viscous Newtonian flows. Continuum Mech. Thermodyn. **28**, p. 85-104, DOI 10.1007/s00161-014-0401-6.

[27] Serre, F. (1953) Contribution à l'étude des écoulements permanents et variables dans les canaux. La Houille blanche, **8**, 830872, 1953.

[28] Toro, E. F. (2013) Riemann solvers and numerical methods for fluid dynamics: a practical introduction. Springer Science and Business Media.

[29] Su, C. H. & Gardner, C. S. (1969) Korteweg - de Vries Equation and Generalisations. III. Derivation of the Korteweg - de Vries Equation and Burgers Equation, J. Math. Physics, **10**, 536–539.

[30] Salmon, R. (1998) Lectures on Geophysical Fluid Mechanics, Oxford University Press, 1998.

[31] Treske, A. (1994) Undular bores (favre-waves) in open channels-experimental studies. Journal of Hydraulic Research, 32(3), 355-370.

[32] Whitham, G. B. (1974) Linear and Nonlinear Waves, John Wiley & Sons.